

# Kinetic characterization of brush border myosin-I ATPase

(unconventional myosin/kinetics)

JAMES D. JONTES<sup>†‡</sup>, RONALD A. MILLIGAN<sup>†</sup>, THOMAS D. POLLARD<sup>§</sup>, AND E. MICHAEL OSTAP<sup>¶||</sup>

<sup>†</sup>Department of Cell Biology, The Scripps Research Institute, La Jolla, CA 92037; <sup>§</sup>Salk Institute for Biological Studies, La Jolla, CA 92037; and <sup>¶</sup>Department of Physiology, University of Pennsylvania School of Medicine, Philadelphia, PA 19104

Contributed by Thomas D. Pollard, October 27, 1997

**ABSTRACT** Brush border myosin-I (BBM-I) is a single-headed unconventional myosin found in the microvilli of intestinal epithelial cells. We used stopped-flow kinetic analysis to measure the rate and equilibrium constants for several steps in the BBM-I ATPase cycle. We determined the rates for ATP binding to BBM-I and brush border actomyosin-I (actoBBM-I), the rate of actoBBM-I dissociation by ATP, and the rates for the steps in ADP dissociation from actoBBM-I. The rate and equilibrium constants for several of the steps in the actoBBM-I ATPase are significantly different from those of other members of the myosin superfamily. Most notably, dissociation of the actoBBM-I complex by ATP and release of ADP from actoBBM-I are both very slow. The slow rates of these steps may play a role in lengthening the time spent in force-generating states and in limiting the maximal rate of BBM-I motility. In addition, release of ADP from the actoBBM-I complex occurs in at least two steps. This study provides evidence for a member of the myosin superfamily with markedly divergent kinetic behavior.

Members of the myosin superfamily constitute a diverse group of molecular motors, which are involved in a wide range of intracellular processes (1, 2). Despite the growing number of unconventional myosins and their potential importance in cell biology, few of these molecules have been characterized in detail. A better understanding of the structural, mechanical, and biochemical properties of myosin family members is important for a variety of reasons. First, characterization of each myosin's properties will help clarify its physiological function. For instance, the distinct physiologies of smooth and skeletal muscles can be explained by the kinetic properties of their myosins (e.g., see refs. 3–5). Comparative analysis will be particularly important for myosins whose cellular functions have not yet been discovered. Second, characterizing a range of myosin types will help improve our understanding of the mechanism of energy transduction by actomyosin. Assuming that the underlying principles of energy transduction are common within the myosin superfamily, identification of differences between myosins should focus attention on those aspects of the myosin enzymatic cycle that are most important.

Brush border myosin-I (BBM-I), a single-headed myosin present in the microvilli of intestinal epithelial cells, links the core bundle of actin filaments to the plasma membrane (6–8). Both the steady-state ATPase and *in vitro* motility activities (9, 10) are very slow compared with those of other myosins (reviewed in refs. 2 and 11). Unexpectedly, cryoelectron microscopy provided evidence that ADP binding causes a large conformational change in BBM-I bound to actin filaments (actoBBM-I) (12, 13). This conformational change was also observed in smooth muscle myosin subfragment 1 (S1) (14) but

not with skeletal muscle S1 (15), raising the question of how BBM-I and smooth muscle S1 differ from skeletal muscle S1.

This study was undertaken to determine the rate and equilibrium constants for several of the important steps in the BBM-I ATPase for comparison to other members of the myosin superfamily, as well as to better understand the cryoelectron microscopy studies (12, 14, 16). The kinetic properties of BBM-I are dramatically different from those of previously characterized myosins. These results have important implications for BBM-I function, for actomyosin mechanochemistry, and for the evolution of the myosin superfamily.

## METHODS

**Proteins and Reagents.** BBM-I was prepared as described in ref. 16, and actin was prepared by the method of Spudich and Watt (17). All experiments were performed in the following buffer: 10 mM imidazole, pH 7.0/50 mM KCl/1 mM DTT/1 mM EGTA/1 mM MgCl<sub>2</sub>. Prior to use, the actin was dialyzed overnight to remove free nucleotide. Pyrene labeling of actin was performed as described (18). 2'(3')-O-(N-Methylanthraniloyl)-ATP (mantATP) (19) was kindly provided by E. W. Taylor (Univ. of Chicago, Chicago). BBM-I concentration was measured by using the BCA protein determination system (Pierce), and the actin concentration was determined by assuming 38.5 μM/A at 290 nm. Pyrene concentration was measured assuming 45.5 μM/A at 344 nm, and the labeled actin was measured as  $[A_{290} - (0.127 \times A_{344})] \times 38.5 \mu\text{M}$  (18). Nucleotide concentrations were measured by using extinction coefficients of  $\epsilon_{259} = 15,400 \text{ M}^{-1}\cdot\text{cm}^{-1}$  for ATP and ADP and  $\epsilon_{255} = 23,300 \text{ M}^{-1}\cdot\text{cm}^{-1}$  for mantATP (14).

**Stopped-Flow Experiments.** Stopped-flow measurements were collected on two instruments, one in Baltimore described in ref. 20, and a KinTek Mark II (KinTek, College Park, PA) at the University of Pennsylvania. For the Baltimore instrument, a 365-nm bandpass filter was used for the excitation and a 410-nm long-pass filter was used for the emission. For the Philadelphia instrument, the excitation wavelength was set to 365 nm with a monochromator and a 400-nm long-pass filter was used for emission. All experiments were performed at 25°C, and all concentrations cited in the text refer to concentrations after mixing.

Curve-fitting and kinetic simulations were performed by using the programs KFIT and KSIM, written by N. Millar (Univ. of California, Los Angeles). The simulations of transients in the presence of ADP were performed in two steps: (i) steady-state concentrations of actoBBM-I-ADP intermediates were determined as a function of ADP concentration, then (ii)

Abbreviations: BBM-I, brush border myosin-I; actoBBM-I, actin bound to BBM-I; AM, actomyosin; S1, myosin subfragment 1; mantATP, 2'(3')-O-(N-methylanthraniloyl)-ATP.

<sup>‡</sup>Present address: Department of Molecular and Cellular Physiology, Stanford University School of Medicine, Stanford, CA 94305.

<sup>||</sup>To whom reprint requests should be addressed at: Department of Physiology, University of Pennsylvania School of Medicine, B400 Richards Building, Philadelphia, PA 19104. e-mail: ostap@mail.med.upenn.edu.

The publication costs of this article were defrayed in part by page charge payment. This article must therefore be hereby marked "advertisement" in accordance with 18 U.S.C. §1734 solely to indicate this fact.

© 1997 by The National Academy of Sciences 0027-8424/97/9414332-6\$2.00/0  
PNAS is available online at <http://www.pnas.org>.

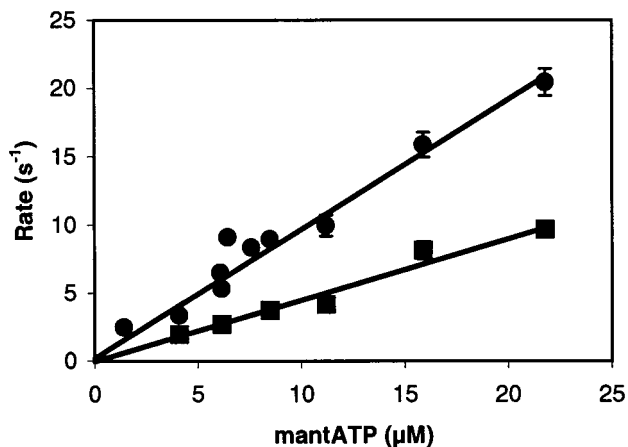
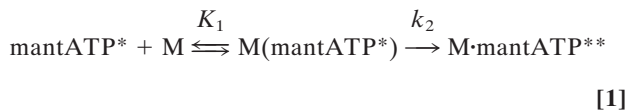


Fig. 1. Rate of mantATP binding to BBM-I (●) and actoBBM-I ■. Each point is the average of 1–5 transients from two protein preparations. The solid lines are the best linear fits through the data points.  $K_1k_2 = 0.95 \pm 0.04 \mu\text{M}^{-1}\cdot\text{s}^{-1}$  for BBM-I.  $K_1'k_2' = 0.45 \pm 0.04 \mu\text{M}^{-1}\cdot\text{s}^{-1}$  for actoBBM-I.

actoBBM-I dissociation transients were simulated as a function of ATP concentration.

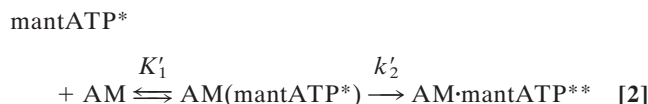
### RESULTS

**mantATP Binding to BBM-I and actoBBM-I.** The enhancement in fluorescence of the ATP analogue mantATP upon binding to myosin (19, 21) allowed us to measure the rate of nucleotide binding to BBM-I. The transient increase in nucleotide fluorescence was best fit to a single exponential at all ATP concentrations examined (Fig. 1). Because of the reduced signal-to-noise ratio at high nucleotide concentrations, we were unable to collect data above  $\approx 25 \mu\text{M}$  mantATP. The binding of mantATP to BBM-I can be described by two steps:



The first step is the formation of a binary collision complex of BBM-I (M) and nucleotide and the second step is a fast isomerization, resulting in enhanced fluorescence of the mantATP (indicated by two asterisks). The apparent second-order rate constant, given by the slope of the plot of observed rate constant vs. nucleotide concentration, is  $K_1k_2 = 0.95 \pm$

$0.04 \mu\text{M}^{-1}\cdot\text{s}^{-1}$  (Fig. 1; Table 1). We also measured the rate of mantATP binding to actoBBM-I (AM), where



At each of the nucleotide concentrations examined, the fluorescence transients were fit by single exponentials. The slope of the plot of  $k_{\text{obs}}$  vs. mantATP concentration yields a value of  $0.45 \pm 0.04 \mu\text{M}^{-1}\cdot\text{s}^{-1}$  for the apparent second-order rate constant,  $K_1'k_2'$  (Fig. 1; Table 1).

**BBM-I Binding to Pyrene-Labeled Actin.** The  $\approx 80\%$  fluorescence quenching upon BBM-I binding to pyrene-actin allowed us to monitor association and dissociation of the actoBBM-I complex (25, 27). The fluorescence signal from the equilibrium binding of BBM-I to  $0.5 \mu\text{M}$  pyrene-actin-phalloidin in the absence of ATP was normalized to the maximum fluorescence intensity (Fig. 2). At a 1:1 ratio of pyrene-actin to BBM-I, all of the myosin is bound. Therefore, the dissociation equilibrium constant ( $1/K_7$ ) is  $< 0.01 \mu\text{M}$  (Fig. 2). Binding is  $\approx 5\times$  tighter than for *Acanthamoeba* myosin-I isoforms (25).

**Dissociation of actoBBM-I by ATP.** We used pyrene fluorescence to monitor the ATP-induced dissociation of actoBBM-I (28). Mixing ATP with pyrene-actoBBM-I resulted in an increase in fluorescence, which was best fit to a single exponential at ATP concentrations  $< 0.1 \text{ mM}$ . The rate of the fluorescence change increased linearly with ATP concentration up to  $50 \mu\text{M}$  under pseudo-first-order conditions (Fig. 2). The mechanism for actoBBM-I dissociation can be defined as



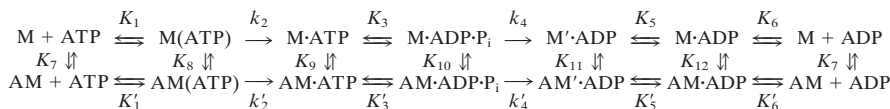
where  $K_1$  is a rapid equilibrium and step 2 is a rate-limiting isomerization to a state of enhanced pyrene-actin fluorescence. This measurement assumes the dissociation steps ( $k_{+9}$  and  $k_{+10}$ , Table 1) are fast, so  $k_2$  limits the rate of dissociation (26, 28). The apparent second-order rate constant ( $K_1'k_2'$ ) is obtained from the slope of the linear region of the curve:  $K_1'k_2' = 0.23 \pm 0.01 \mu\text{M}^{-1}\cdot\text{s}^{-1}$  (Fig. 2).

At ATP concentrations  $> 0.1 \text{ mM}$ , the transient change in pyrene fluorescence sometimes deviated from a single exponential rate. A second slow phase ( $20 \text{ s}^{-1}$ ) with a small and variable amplitude (0–15%) was detected. Although the amplitude of this phase varied throughout our investigation, it

Table 1. Summary of BBM-I rate and equilibrium constants

Step	BBM-I	Skeletal myosin	Smooth myosin	<i>Acanthamoeba</i> myosin-IA
$K_1k_2, \mu\text{M}^{-1}\cdot\text{s}^{-1}$	0.95	5.6*	3.2*	0.74 <sup>¶</sup>
$K_1'k_2', \mu\text{M}^{-1}\cdot\text{s}^{-1}$	0.45	8.0*	2.0*	—
	0.32	3.0 <sup>‡</sup>	—	0.29 <sup>¶</sup>
$k_2', \text{s}^{-1}$	200	$>1,500^*$	1,300*	$>300^{\parallel}$
$k_5, \text{s}^{-1}$	0.18	0.22 <sup>‡</sup>	—	—
$k_{+5}, \text{s}^{-1}$	8	$\approx 325^{\parallel}$	—	—
$k_{-5}, \text{s}^{-1}$	13	—	—	—
$K_5'$	0.62	$>50^{\S}$	—	—
$K_6, \mu\text{M}$	11	200 <sup>†</sup>	—	53 <sup>¶</sup>

Constants are as in the following scheme, in which M is myosin and AM is actomyosin:



Data are from the following sources: \*, ref. 22; †, ref. 23; ‡, ref. 21; §, ref. 24; ¶, ref. 25; and ||, ref. 26.

remained constant for a given experiment and is most likely due to a small ADP contamination (0–500 nM; see below). The variable slow phase was not included in the analysis of ATP-induced actoBBM-I dissociation.

The rate of dissociation of BBM-I from pyrene-actin-phalloidin over a range of ATP concentrations from 0.10 to 2.2 mM is not linear (Fig. 2), but can be fit to an hyperbola as described (26):

$$k_{\text{obs}} = K'_1 k'_2 [\text{ATP}] / (K'_1 [\text{ATP}] + 1) \quad [4]$$

yielding a value of  $1.6 \times 10^3 \pm 300 \text{ M}^{-1}$  for  $K'_1$  and  $200 \pm 19 \text{ s}^{-1}$  for  $k'_2$ . The apparent second-order rate constant ( $K'_1 k'_2$ ) calculated from the values of  $K'_1$  and  $k'_2$  ( $0.32 \pm 0.07 \mu\text{M}^{-1}\text{s}^{-1}$ ) is faster than the value determined from the initial slope of the plot. While the value of  $K'_1$  is similar to values determined for other myosins (22), the value of  $k'_2$  is 1/5 of that for previously characterized myosin isoforms.

**ADP Dissociation from BBM-I.** We measured the rate of ADP release from BBM-I by displacing mantADP from BBM-I with excess ATP. In the presence of excess ATP, the rate of fluorescence decay is determined by the rate of ADP dissociation ( $k_6$ ) as described by

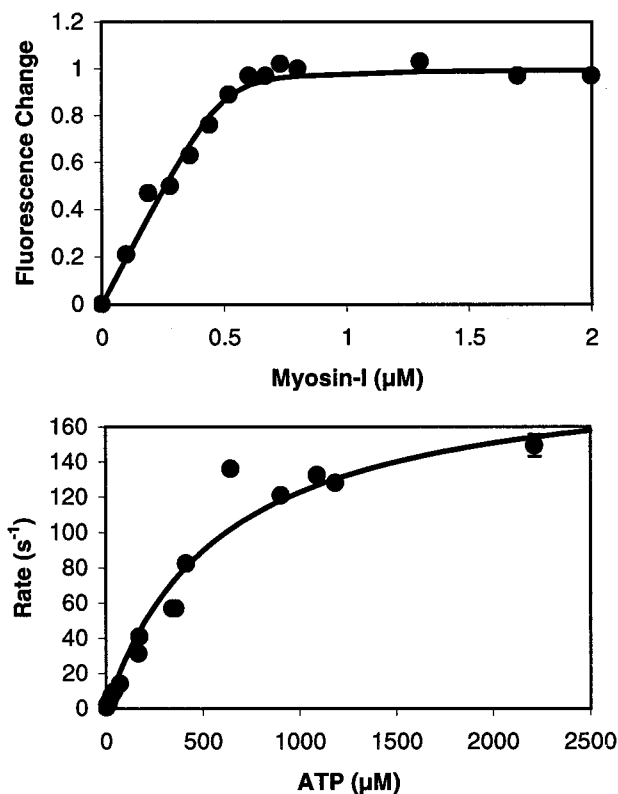
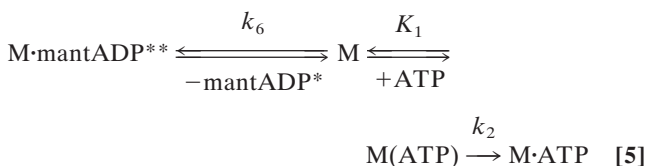
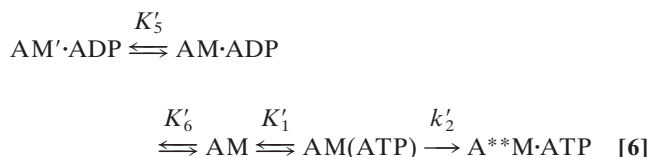


FIG. 2. (Upper) Fluorescence titration of  $0.5 \mu\text{M}$  pyrene-actin-phalloidin with BBM-I. Maximum quenching of fluorescence by BBM-I is plotted as 1.0. The solid line is a fit as described in the text:  $1/K_7 < 0.01 \mu\text{M}$ . (Lower) Rate of ATP-induced dissociation of BBM-I from pyrene-actin-phalloidin as a function of nucleotide concentration. Each data point is the average of 1–5 transients from three protein preparations. The solid line is a fit to Eq. 5 as described in the text:  $K'_1 = 1.6 \times 10^3 \pm 300 \text{ M}^{-1}$  and  $k'_2 = 200 \pm 19 \text{ s}^{-1}$ .

BBM-I ( $0.5 \mu\text{M}$ ) was incubated with  $30 \mu\text{M}$  mantADP and mixed with  $500 \mu\text{M}$  ATP. The rate of fluorescence decay of mantADP was best fit by a single exponential with a rate constant of  $0.18 \text{ s}^{-1}$  (data not shown). Although we did not determine the equilibrium constant for mantADP binding ( $K_6$ ), skeletal muscle S1 would be saturated with mantADP under the experimental concentrations (21). The fluorescence of mantADP-actoBBM-I did not change after mixing with ATP, suggesting that the structure of the nucleotide binding pocket of BBM-I is different when bound to actin (data not shown).

**ADP Dissociation from actoBBM-I.** We measured the rate of ADP dissociation from the ternary actoBBM-I-ADP complex from the rate of enhancement of pyrene fluorescence when ATP dissociated BBM-I from pyrene-actin-phalloidin (25, 28). In the presence of excess ATP, the dissociation of BBM-I from actin should be limited by the rate of ADP release as described by



If the AM and AM·ADP states are in a rapid equilibrium ( $K'_6$ ), and AM'·ADP is not populated, (i) the increase in pyrene

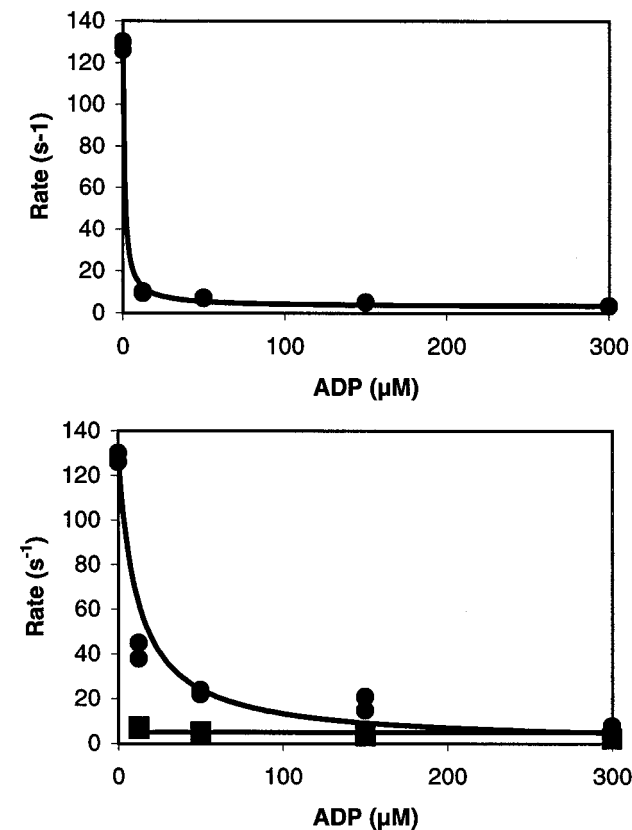


FIG. 3. Dependence of the rate of  $1.2 \text{ mM}$  ATP binding to a  $0.5 \mu\text{M}$  complex of pyrene-actin-phalloidin-BBM-I on the concentration of ADP. (Upper) The observed first-order rate constants at each ADP concentration were obtained by fitting the stopped-flow data to a single exponential. The solid line is a fit to Eq. 7 as described in the text:  $K'_6 = 1.0 \mu\text{M}$ . (Lower) Experimental transients at each ADP concentration were fit to two exponential rates. The rate of the slow component ( $k_{\text{obs1}}$ , ■) is defined by  $k'_5$ , and the rate of the fast component ( $k_{\text{obs2}}$ , ●) is defined by  $k'_6$  and the ADP concentration. The solid line through the circles is a fit to Eq. 8 as described in the text.

fluorescence will be a single exponential, and (ii) the dependence of  $k_{\text{obs}}$  on ADP concentration will be

$$k_{\text{obs}} = k_0(1 + [\text{ADP}]/K'_6) \quad [7]$$

where  $k_{\text{obs}}$  is the observed dissociation rate,  $k_0$  is the dissociation rate in the absence of ADP, and  $K'_6$  is the dissociation equilibrium constant for ADP (25, 29). We measured the rate of ADP release from actoBBM-I at five ADP concentrations for each of four ATP concentrations. The addition of ADP to actoBBM-I in the absence of ATP did not change the pyrene-actin fluorescence. We fit the time course of the fluorescence increase due to the ATP-induced dissociation of the pyrene actoBBM-I to a single exponential and plotted the rate vs. the ADP concentration (Fig. 3). Nonlinear least-square fits to the data yield a  $K'_6$  value of  $1.0 \mu\text{M}$  (Fig. 3). However, the experimental transients were not fit adequately by a single exponential, but were best fit by two exponentials as determined by examination of residuals (Fig. 4) and the calculation of  $\chi^2$ . Unlike the pyrene-actin BBM-I dissociation transients, the appearance of the second exponential was not variable, and the relative amplitudes of the exponentials depended directly on the ADP concentration.

We plotted the rates from the two-exponential fits vs. ADP concentration (Fig. 3). Whereas the slow rate ( $k_{\text{obs}1}$ ) is relatively insensitive to the ADP concentration under the concentrations tested ( $k_{\text{obs}1} = 3\text{--}7 \text{ s}^{-1}$ ), the rate and amplitude of the faster of the two exponentials ( $k_{\text{obs}2}$ ) decreases with increasing ADP. This biphasic behavior suggests the presence of two AM·ADP states (Eq. 6) with  $k_{\text{obs}1}$  defined by step 5 and  $k_{\text{obs}2}$  related to the ADP concentration by (24, 26, 30, 31)

$$k_{\text{obs}2} = K'_1 k'_2 [\text{ATP}] / (1 + K'_1 [\text{ATP}] + [\text{ADP}] / K'_6). \quad [8]$$

Nonlinear least-square fits to the data acquired at 0.9 mM, 1.2 mM, and 2.2 mM ATP yield a  $K'_6$  value of  $4 \mu\text{M}$  when  $K'_1$  is  $1.6 \times 10^3 \text{ M}^{-1}$  and  $k_2 = 200 \text{ s}^{-1}$  (Fig. 3).

We determined  $K'_5$ ,  $k'_{+5}$ , and  $k'_{-5}$  by fitting experimental transients at different ADP concentrations to kinetic simulations (Eq. 6; Fig. 5). The simulated transient reports the transient population of the A\*\*M·ATP state. Simulations

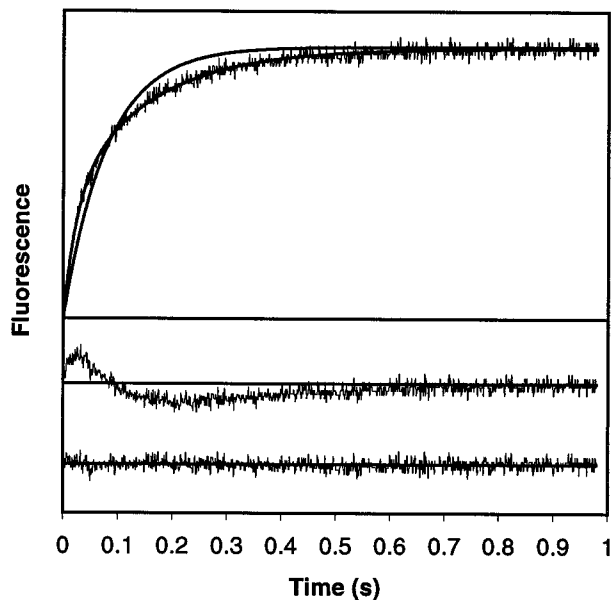


FIG. 4. Stopped-flow fluorescence transients showing the dissociation of  $0.5 \mu\text{M}$  BBM-I from pyrene-actin-phalloidin by  $1.2 \text{ mM}$  ATP in the presence of  $12.5 \mu\text{M}$  ADP. Solid lines show single- and double-exponential fits to the data. Residuals obtained by subtracting the experimental data from the single-exponential fit (Middle) and the double-exponential fit (Bottom) are shown.

indicate that the relative amplitudes of the two exponentials at a given ADP concentration depend directly on  $K'_5$ . As  $K'_5$  decreases, the amplitude of the  $k_{\text{obs}1}$  increases. This dependence allowed us to determine the value of  $K'_5$ . Iterative manual simulations using the fixed values  $K'_1 = 1.6 \times 10^3 \text{ M}^{-1}$  and  $k'_2 = 200 \text{ s}^{-1}$  yielded the following constants:  $k'_{+5} = 8 \text{ s}^{-1}$ ,  $k'_{-5} = 13 \text{ s}^{-1}$ ,  $K'_5 = 0.62$ , and  $K'_6 = 11 \mu\text{M}$  (Fig. 5). Varying the values of  $K'_1$  and  $k'_2$  by a factor of 2 did not significantly alter the fit as long as  $K'_1 k'_2 = 0.32 \mu\text{M}^{-1} \text{ s}^{-1}$ . It is important to note that  $K'_6$  is modeled as a rapid equilibrium step. However, this may be an over-simplification. It is possible that  $k'_{+6}$  may be slow enough to limit the rate of ADP release, complicating our kinetic analysis. Direct measurements of the rate and equilibrium constant for ADP binding are required to further test our model.

The calculated rate constants indicate that the AM·ADP state is significantly populated at equilibrium in the presence of micromolar ADP. This differs from skeletal muscle myosin-II and *Acanthamoeba* myosin-I, and may explain why large-scale ADP-induced structural changes are observed with BBM-I, but not with skeletal muscle myosin-II.

## DISCUSSION

**Overview of the BBM-I ATPase Cycle.** The apparent second-order rate constant for ATP-induced actoBBM-I dissociation obtained from the slope of the linear region of Fig. 2 ( $0.23 \pm 0.01 \mu\text{M}^{-1} \text{ s}^{-1}$ ) is significantly slower than that obtained by (i) fitting the entire curve to Eq. 4 ( $0.32 \pm 0.07 \mu\text{M}^{-1} \text{ s}^{-1}$ ) or, (ii) fitting the ADP release data (Fig. 5) to Eq. 6. This difference is most likely due to a small ADP contamination that is not resolved at low ATP concentrations. Using the rate constants determined from fitting the ADP release data (Eq. 6; Fig. 5), we determined that a  $500 \text{ nM}$  ADP contamination would result in an apparent second-order rate constant of  $0.24 \mu\text{M}^{-1} \text{ s}^{-1}$  for actoBBM-I dissociation.

The apparent second-order rate constant for the binding of mant-ATP to actoBBM-I is  $K'_1 k'_2 = 0.45 \pm 0.04 \mu\text{M}^{-1} \text{ s}^{-1}$  (Fig. 1). The difference in  $K'_1 k'_2$  measured by mantATP binding and by pyrene-actoBBM-I dissociation is likely due to the effect of pyrene labeling of actin, which reduces the rate of actomyosin-II dissociation (31).

Dissociation of actoBBM-I by ATP occurs with an apparent second-order rate constant of  $0.32 \mu\text{M}^{-1} \text{ s}^{-1}$ , reaching a maximal rate of  $200 \text{ s}^{-1}$  (Fig. 2). The maximal rate of dissociation is  $> 5$ -fold slower than that of skeletal muscle myosin-II

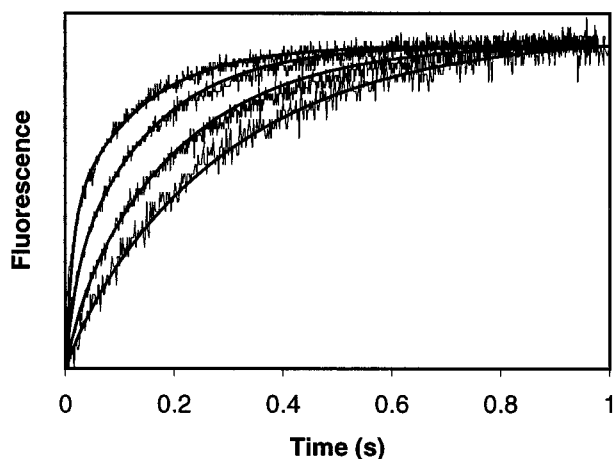


FIG. 5. Stopped-flow fluorescence transients showing the dissociation of  $0.5 \mu\text{M}$  BBM-I from  $0.5 \mu\text{M}$  pyrene-actin-phalloidin by  $1.2 \text{ mM}$  ATP in the presence of  $12.5$ ,  $50$ ,  $150$ , and  $300 \mu\text{M}$  ADP (top to bottom, respectively). Solid lines show simulated transients to Eq. 6 calculated as described in the text.

(22, 32), so under physiological ATP conditions ( $\approx 1$  mM), actoBBM-I dissociates at a rate of  $\approx 200$  s<sup>-1</sup> and actomyosin-II dissociates at a rate of  $\approx 1,000$  s<sup>-1</sup>.

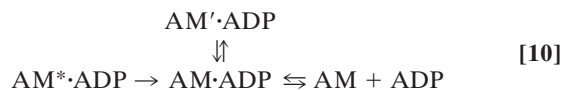
Dissociation of ADP from actoBBM-I is a two-step process as described by Eq. 6. The first step is a first-order isomerization ( $k'_{+5} + k'_{-5} = 21$  s<sup>-1</sup>;  $K'_5 = 0.6$ ) of the strongly bound actoBBM-I·ADP complex (AM'·ADP) to a second strongly bound state (AM·ADP) that is in rapid equilibrium ( $K'_6 = 10$  μM) with a nucleotide-free state (AM). A similar two-step ADP release pathway has been proposed for skeletal muscle myosin-II (24, 26, 30, 31, 33). However,  $K'_5$  for skeletal muscle myosin-II is estimated to be  $>50$ , and  $k'_{+5} + k'_{-5}$  is  $> 100$  s<sup>-1</sup> (24, 31). Therefore, at high ATP concentrations during steady-state ATP hydrolysis by BBM-I, we predict the lifetime of the force-producing states (AM'·ADP and AM·ADP) to be greater than 50 ms. Low concentrations of ADP will increase the lifetime of these states dramatically. This is significantly longer than the  $\approx 5$ -ms lifetime reported for the population of the force-producing states of skeletal muscle myosin-II (34).

Because all of the rate constants that we determined are faster than the steady-state ATPase rate (0.3 s<sup>-1</sup>), the rate-limiting step must occur between actoBBM-I dissociation and ADP release. The same is true for myosin-II (22, 23, 35, 36) and for amoeba myosin-I (25). The most likely candidate for this slow step is phosphate release ( $k'_4$ ) or an isomerization preceding phosphate release. This step is proposed to regulate the transition between the weak-binding (non-force-bearing) and strong-binding (force-bearing) states in the myosin-II ATPase cycle (25, 37). While it remains possible that ATP hydrolysis is rate limiting, previous investigations of other myosins indicate it is unlikely (26, 32).

**ADP Release and Its Relationship to Structural Studies.** It can be argued that the AM'·ADP state observed in this investigation is an additional state, unique to BBM-I and having no analog in the skeletal muscle myosin-II ATPase pathway. Such a hypothesis suggests that BBM-I retains the AM·ADP isomerization step with  $K'_5 > 50$ . This remains a formal possibility, because we have not proven that our AM'·ADP state is identical to that of Sleep and Hutton (24), and we did not detect a change in pyrene-actin fluorescence upon ADP binding (29). Two alternative schemes are presented below:



or



where AM\*·ADP is the state defined by others (24, 29, 31) and AM'·ADP is the state we defined for BBM-I. Although the most direct interpretation of our data is to equate the AM'·ADP state we observe with that of Sleep and Hutton (24) and Taylor (31), additional experiments are required to test this hypothesis rigorously.

ADP release ( $K'_6$ ) is best modeled as a rapid equilibrium step for skeletal muscle (26) and cytoplasmic (35) myosin-II with  $K_d$  values of 120 μM and 94 μM, respectively, and the actual rate of ADP release for skeletal muscle myosin-II is  $> 300$  s<sup>-1</sup>. However, the ADP dissociation equilibrium constant for smooth muscle myosin-II ( $K_d = 10$  μM; H. L. Sweeney, personal communication) is of the same order as BBM-I (apparent  $K_d \approx 1$  μM), as is the effective rate of ADP release (30–70 s<sup>-1</sup>; H. L. Sweeney, personal communication). It is plausible to suggest that the slow rate of ADP release by smooth muscle myosin-II is also due to the steady-state population of two AM·ADP states. We tentatively propose that a high affinity for ADP (apparent  $K_d < 5$  μM), and a

steady-state population of two AM·ADP states, may be diagnostic of the ADP-induced conformation change (i.e., 3- to 6-nm movement of the light chain domain) observed for both smooth muscle S1 (14) and for BBM-I (12, 16). This idea is consistent with the observation that skeletal muscle myosin-II does not exhibit an ADP-dependent movement (ref. 15; R. Diaz and R.A.M., unpublished observations). It has been suggested that the smooth muscle "latch" state is due to a high affinity of smooth muscle myosin for ADP in combination with the accumulation of ADP during contraction (3, 5). Our data suggest that the effect of ADP on BBM-I (and possibly smooth muscle S1) could be to populate a second, higher-affinity AM'·ADP state. Although it is possible that such an AM'·ADP state could be a peculiar state unique to these myosins, it seems more likely that the property is simple due to the kinetic variations on a common underlying theme.

**Relevance of BBM-I Kinetics to *In Vivo* Function.** ATP-induced actoBBM-I dissociation and ADP release are much slower than in myosin-II and *Acanthamoeba* myosin-I, but these steps are much faster than the steady-state turnover rate ( $\approx 0.3$  s<sup>-1</sup> at 25°C). Despite the remarkably long lifetimes of key strong-binding intermediates (AM, AM·ADP), ATP-induced actomyosin dissociation and ADP release contribute 5–10% of the total ATPase cycle for both myosin-II and BBM-I. Therefore, in the absence of an external load, the predominant steady-state intermediates for all characterized myosins are weakly bound to or detached from the actin filament. This is referred to as a small duty cycle. However, the locally high concentration of BBM-I in the microvillus [ $> 70$  μM (38, 39)] ensures that a significant fraction of the BBM-I remains bound to actin during the ATPase cycle.

**What Is the Physiological Significance of the Slow Actin-Activated ATPase Rate of BBM-I?** Cell biological evidence suggests that BBM-I transports Golgi-derived vesicles through the highly crosslinked terminal web to the apical membrane in both developing and mature enterocytes (40). The average cytoplasmic pore size is smaller than these vesicles (40, 41). If the enzymatic and translational rate of the vesicle motor were the same as that of skeletal muscle myosin-II (10–20 s<sup>-1</sup>; 10 μm/s), the cell cortex would seem inelastic, and the actin in the cell cortex would have to be severed or opened to allow the vesicle to pass to the membrane (42). However, because the rate constants that define the enzymatic and translational rate of BBM-I are on the same order as the dissociation rate of cytoskeletal crosslinkers (43), the vesicle can move slowly through the terminal web without compromising the structural integrity of the cell cortex.

The long lifetimes of the actin-bound intermediates may also be critical for the proposed structural role of BBM-I as a dynamic crosslinker between the membrane and actin filaments in the microvillus. At high rates of externally imposed force, the crosslinks would be stiff, allowing the microvillus to resist deformation. However, a change in shape would be possible if the rate of imposed force was slower than the lifetime of the strongly bound states.

**What Is the Physiological Significance of Two ADP States?** It is likely that the 6-nm movement of the BBM-I regulatory domain observed upon ADP release (12, 13) is a structural transition that accompanies the biochemical transition between ADP states ( $k'_5$ ; Eq. 6). While it is unlikely that this step is the entire power stroke observed in skeletal muscle fibers (12, 29, 33), it is possible that the power stroke occurs in two steps, one preceding phosphate release (44) and one preceding ADP release ( $k'_5$ ; ref. 12). However, it is also possible that this transition is a "force-sensing" step, responsible for limiting the ATPase and actin-detachment rates in cases of high strain or high ADP concentration, much like the proposed strain-dependent step of myosin-II (45, 46). After undergoing its power-stroke, BBM-I may require an additional 6-nm step before ADP is released. When the crossbridge is strained, the

6-nm step is blocked and the cycle will not be completed. The presence of a force-sensing step has implications for several processes, including a "latch" state (3, 5, 14), movement of vesicles through the dense cytoplasm, and—perhaps most intriguing—processivity. Further investigations that rigorously correlate structural (12, 47), biochemical, and force-producing (34) properties are required to test this hypothesis.

This work was initiated at The Johns Hopkins University School of Medicine. We thank E. W. Taylor for providing the mantATP used in this study and for a critical review of this manuscript. We also thank A. Weber for a donation of pyrene-labeled actin, and H. L. Sweeney and E. De La Cruz for stimulating discussions. This work was supported by research grants from the National Institutes of Health (AR-39155 and AR-44278 to R.A.M. and GM-26132 to T.D.P.). R.A.M. is an established investigator of the American Heart Association. E.M.O. was supported by a grant from the Cancer Research Fund of the Damon Runyon–Walter Winchell Foundation Fellowship (DRG-1294) and by a McCabe Fund Pilot-Project Award. J.D.J. was supported by a predoctoral fellowship from the Howard Hughes Medical Institute.

1. Mooseker, M. S. & Cheney, R. E. (1995) *Annu. Rev. Cell Dev. Biol.* **11**, 633–675.
2. Sellers, J. R. & Goodson, H. V. (1995) *Protein Profile* **2**, 1323–1423.
3. Drew, J. S., Harwalkar, V. A. & Stein, L. A. (1992) *Circ. Res.* **71**, 1067–1077.
4. Guilford, W. H., Dupuis, D. E., Kennedy, G., Wu, J., Patlak, J. B. & Warshaw, D. M. (1997) *Biophys. J.* **72**, 1006–1021.
5. Nishye, E., Somlyo, A. V., Török, K. & Somlyo, A. P. (1993) *J. Physiol.* **460**, 247–271.
6. Hoshimaru, M. & Nakanishi, S. (1987) *J. Biol. Chem.* **262**, 14625–14632.
7. Howe, C. L. & Mooseker, M. S. (1983) *J. Cell Biol.* **97**, 974–985.
8. Matsudaira, P. T. & Burgess, D. R. (1979) *J. Cell Biol.* **83**, 667–673.
9. Collins, K., Sellers, J. R. & Matsudaira, P. (1990) *J. Cell Biol.* **110**, 1137–1147.
10. Wolenski, J. S., Hayden, S. M., Forscher, P. & Mooseker, M. S. (1993) *J. Cell Biol.* **122**, 613–621.
11. Pollard, T. D., Doberstein, S. K. & Zot, H. G. (1991) *Annu. Rev. Physiol.* **53**, 653–681.
12. Jontes, J. D. & Milligan, R. A. (1997) *J. Cell Biol.* **139**, 683–693.
13. Jontes, J. D., Wilson-Kubalek, E. M. & Milligan, R. A. (1995) *Nature (London)* **378**, 751–753.
14. Whittaker, M., Wilson-Kubalek, E. M., Smith, J. E., Faust, L., Milligan, R. A. & Sweeney, H. L. (1995) *Nature (London)* **378**, 748–751.
15. Gollub, J., Cremona, C. R. & Cooke, R. (1996) *Nat. Struct. Biol.* **5**, 351–361.
16. Jontes, J. D. & Milligan, R. A. (1997) *J. Mol. Biol.* **266**, 331–342.
17. Spudich, J. A. & Watt, S. (1971) *J. Biol. Chem.* **246**, 4866–4871.
18. Pollard, T. D. (1984) *J. Cell Biol.* **99**, 769–777.
19. Hiratsuka, T. (1983) *Biochim. Biophys. Acta* **742**, 496–508.
20. Sinard, J. H. & Pollard, T. D. (1990) *J. Biol. Chem.* **265**, 3654–3660.
21. Woodward, S. K. A., Eccleston, J. F. & Geeves, M. A. (1991) *Biochemistry* **30**, 422–430.
22. Marston, S. & Taylor, E. W. (1980) *J. Mol. Biol.* **139**, 573–600.
23. White, H. D. (1977) *Biophys. J.* **17**, 40a.
24. Sleep, J. A. & Hutton, R. L. (1980) *Biochemistry* **19**, 1276–1283.
25. Ostap, E. M. & Pollard, T. D. (1996) *J. Cell Biol.* **132**, 1053–1060.
26. Ma, Y.-Z. & Taylor, E. W. (1994) *Biophys. J.* **66**, 1542–1553.
27. Geeves, M. A. & Jeffries, T. E. (1988) *Biochem. J.* **256**, 41–46.
28. Criddle, A. H., Geeves, M. A. & Jeffries, T. (1985) *Biochem. J.* **232**, 343–349.
29. Geeves, M. A. (1989) *Biochemistry* **28**, 5864–5871.
30. Shriver, J. W. & Sykes, B. D. (1981) *Biochemistry* **20**, 2004–2012.
31. Taylor, E. W. (1991) *J. Biol. Chem.* **266**, 294–302.
32. Lynn, R. & Taylor, E. W. (1971) *Biochemistry* **10**, 4617–4624.
33. Trybus, K. M. & Taylor, E. W. (1982) *Biochemistry* **21**, 1284–1294.
34. Finer, J. T., Mehta, A. D. & Spudich, J. A. (1995) *Biophys. J.* **68**, 291–297s.
35. Ritchie, M. D., Geeves, M. A., Woodward, S. A. & Manstein D. J. (1993) *Proc. Natl. Acad. Sci. USA* **90**, 8619–8623.
36. White, H. D. & Taylor, E. W. (1976) *Biochemistry* **15**, 5818–5826.
37. Eisenberg, E. & Greene, L. E. (1980) *Annu. Rev. Physiol.* **42**, 293–309.
38. Bretscher, A. (1991) *Annu. Rev. Cell Biol.* **7**, 337–374.
39. Zot, H. G. (1995) *Cell Motil. Cytoskel.* **30**, 26–37.
40. Fath, K. R. & Burgess, D. R. (1993) *J. Cell Biol.* **120**, 117–127.
41. Luby-Phelps, K. Castle, P. E., Taylor, L. & Lanni, F. (1987) *Proc. Natl. Acad. Sci. USA* **84**, 4910–4913.
42. Sato, M., Schwarz, W. & Pollard, T. D. (1987) *Nature (London)* **325**, 828–830.
43. Wachsstock, D. H., Schwarz, W. H. & Pollard, T. D. (1994) *Biophys. J.* **66**, 801–809.
44. Dantzig, J. A., Goldman, Y. E., Millar, N. C., Lackett, J. & Homsher, E. (1992) *J. Physiol.* **451**, 247–278.
45. Huxley, A. F. (1957) *Prog. Biophys. Biophys. Chem.* **7**, 255–318.
46. Huxley, A. F. & Simmons, R. M. (1971) *Nature (London)* **233**, 533–538.
47. Rayment, I., Rypniewski, W. R., Schmidt-Base, K., Smith, R., Tomchick, D. R., Benning, M. M., Winkelmann, D. A., Wesenberg, G. & Holden, H. M. (1993) *Science* **261**, 50–58.